Analysis and design of a single layer double square slot frequency selective surface with single stopband between double passbands

Ji-Song Pae,[1] Song-Jin Im,[1,*] Yong-Ha Han,[1] and Kil-Song Song[1]

[1] *Department of Physics, Kim Il Sung University,*
Taesong District, 02-381-4410 Pyongyang,
Democratic People's Republic of Korea

Abstract

Square loop and square slot are the simplest and commonly used elements of frequency selective surfaces (FSSs) providing bandstop and bandpass responses, respectively. Despite it is already known that employment of a double square slot structure presents a tunable stopband between two passbands, it is not clear which parameters of the structure are crucial for tunning the inbetween stopband. We propose an analysis of a double square slot FSS considering its element as a parallel connection of square slot and square loop predicting two geometrical parameters of the constituent square loop are crucial for tunning the inbetween stopband. The stopband is tunable by changing geometrical parameters of the constituent square loop and does not depend on geometries of the constituent square slot. The validity of this analytical prediction is verified by full wave EM simulation results.

* sj.im@ryongnamsan.edu.kp

I. INTRODUCTION

Recently, frequency selective surfaces (FSSs) have drawn extensive attention due to the widespread applications ranging from microwave systems and antennas to 5G communications. They are electromagnetic filters that exhibit total reflection or transmission over a certain frequency band to an incident electromagnetic wave [1]. With the rapid development of wireless communication technology, the demand for a dual-band FSS has been increased [2]. Many studies to obtain a dual-band frequency response were published [3–14]. In [3], the FSS consisting of closed loop and its complementary pattern was presented. In [5–7] dual-band FSSs with miniaturized elements taking advantages for FSS size reduction and better angular stability were presented and in [8–10, 14] multi-layered dual-band FSSs based on cascading technology were presented. Dual-band FSSs using fractal element and a novel 3-D dual-band FSS having better performance and more flexibility compared to the traditional 2-D FSSs were also reported [11–13].

Square loop and square slot are the simplest and commonly used elements of frequency selective surfaces (FSSs) providing bandstop and bandpass responses, respectively [15–23]. The responses of square loop and square slot FSSs have been well analyzed by using an equivalent circuit approach giving insight into the working principles [3, 23–33]. Double square loop FSSs have been proposed for a dual-band bandstop response in many paper [27, 34–37]. There, the double square loop structure was analyzed as a parallel connection of two different square loops corresponding to two different stopbands. While the analytical results were well known for double square loop structure, analytical models for the double square slot FSS were rarely reported. In [38–40], the dual-band bandpass response of double square slot FSSs [38, 39] and double annular ring slot FSSs [40] were shown only by full wave simulation results and no anlaytical model was suggested. There, the dual passbands were attributed to the double slots, respectively, and two different slot sizes were suggested to be key parameters for tuning the dual passbands. Furthermore, despite it is already known that employment of a double square slot structure presents a tunable stopband between two passbands, it is not clear which parameters of the structure are crucial for tunning the inbetween stopband. It is promising to provide an analysis model for giving insight into the working principles and design guidance for tuning the frequency response of the double square slot. We propose an analysis model for a double square slot metasurface considering

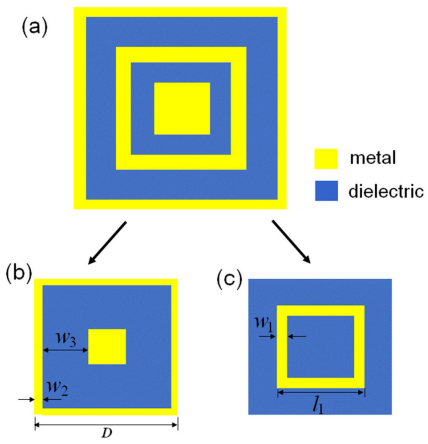

FIG. 1. Geometries of the unit cell of a double square slot metasurface (a) and its constituent square slot (b) and square slot (c).

its element as a parallel connection of square slot and square loop by using the equivalent circuit approach. Our analysis predicts that two geometrical parameters of the constituent square loop are crucial for tunning the inbetween stopband.

II. GEOMETRY AND ANALYTICAL MODEL

The unit cell geometry of the proposed double square slot metasurface is depicted in fig. 1(a). Although the unit cell has a form of double concentric square slots with two different slot sizes, it cannot be decomposed into two different square slots, instead it can be decomposed into the constituent square slot as shown in Fig. 1(b) and the constituent square loop as shown in Fig. 1(c). D is a period of the unit cell, l_1 and w_1 are length and strip width of the square loop, respectively. w_2 and w_3 are strip width and slot width of the square slot, respectively. Now, we construct an equivalent circuit model of the double square slot metasurface as a parallel circuit between the equivalent circuit of the constituent square slot and that of the constituent square loop as shown in Fig. 2(a). Equivalent circuit of the square slot is represented as a parallel L_1C_1 resonator and that of the square loop is represented as a series L_2C_2 resonator. Here, L_1 and C_1 are the equivalent inductance and capacitance of the square loop, respectively. L_2 and C_2 are the equivalent inductance and capacitance of the square slot, respectively. From the equivalent circuit shown in Fig. 2 (a), the complex transmission coefficient S_{21} of the proposed structure is expressed as follows:

$$S_{21} = \frac{2}{2 + (1/Z_1 + 1/Z_2)},$$
$$Z_1 = [j\omega L_1 + 1/(j\omega C_1)]/Z_0,$$
$$Z_2 = [j\omega L_2/(1 - \omega^2 L_2 C_2)]/Z_0, \tag{1}$$

where Z_0 is the vacuum impedance and ω is the operating angular frequency. Fig. 2(b) shows simulation and equivalent circuit model results for frequency response of the double square slot FSS. The equivalent circuit inductance and capacitance values are calculated from the simulation results via the least square curve-fitting process. As can be seen, the transmission spectra has dual passbands and a single stopband. f_{p1} and f_{p2} are lower and upper bandpass frequencies, respectively in which perfect transmission is implemented and f_s is a bandstop frequency in which zero transmission occurs. We now explore explicit expression for f_{p1}, f_{p2} and f_s. From Eq. (1), we can get the resonance conditions $Z_1 + Z_2 = 0$ for perfect transmission and $Z_1 = 0$ or $Z_2 = 0$ for zero transmission. From these resonance conditions and Eq. (1), three resonant frequencies aforementioned in Fig. 2 b) can be derived:

$$f_s = 1/\left(2\pi\sqrt{L_1 C_1}\right), \tag{2}$$

$$f_{p1} = \frac{1}{2\pi}\left(\frac{B + \sqrt{B^2 - 4A}}{2A}\right)^{1/2},$$
$$f_{p2} = \frac{1}{2\pi}\left(\frac{B - \sqrt{B^2 - 4A}}{2A}\right)^{1/2}, \tag{3}$$

where $A \equiv L_1 L_2 C_1 C_2$, $B \equiv L_1 C_1 + L_2 C_1 + L_2 C_2$. As seen in Eq. (2), the bandstop frequency is dependent only on the circuit parameters L_1 and C_1 of the constituent square loop, and is not dependent on the other circuit parameters. However, Eq. (3) shows that the bandpass frequencies are dependent on the circuit parameters of both the constituent square loop and the constituent square slot. Then L_1 and C_1 are controllable by changing geometrical parameters of the square loop [41],

$$L_1 = \mu_0 \frac{l_1}{2\pi} \ln\left(\frac{1}{\sin(\pi w_1/2D)}\right), \tag{4}$$

$$C_1 = \varepsilon_0 \varepsilon_{\text{eff}} \frac{2l_1}{\pi} \ln\left(\frac{1}{\sin(\pi(D - l_1)/2D)}\right), \tag{5}$$

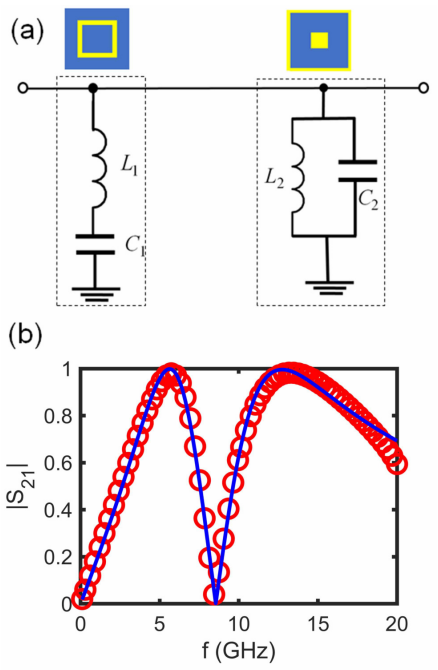

FIG. 2. (a) Equivalent circuit model and (b) transmission spectra of the double square slot metasurface. In (b), the red circles are simulation results and the blue curve has been obtained by using Eq. (1) where the circuit parameters L_1=7.61×10^{-9} H, C_1=4.55×10^{-14} F, L_2=5.44×10^{-9} H and C_2=5.81×10^{-14} F have been calculated the simulation results via the least square curve-fitting process.

where ε_0 , μ_0 are the permittivity and permeability in free space, respectively, and ε_{eff} is the effective permittivity of the structure. Here, Eqs. (4) and (5) describe the individual inductance and capacitance of the constituent square loop neglecting the mutual coupling effect. They are deviated from the inductance and capacitance values considering the mutual effect, however, it is desirable to use these formulas for suggesting what are the key parametrs for tuning the stopband. We note that in our model the mutual effect can be easily incorporated into L_1, C_1, L_2 and C_2. The incorporation of the mutual effect in our analysis model is guaranteed by well agreement between the simulation results and the fitting curve from our analysis model as shown in Fig. 2(b). As seen in Eqs. (4) and (5), L_1 is determined by the length l_1 and the strip width w_1 of the constituent square loop and C_1 is determined only by l_1 when the unit cell period D is fixed. L_1 decreases slightly with the increase of w_1 and, L_1 and C_1 increase significantly with the increase of l_1 . Thus, manipulation of the stopband can be achieved by changing the strip width w_1 and the length l_1 of the square loop. Then,

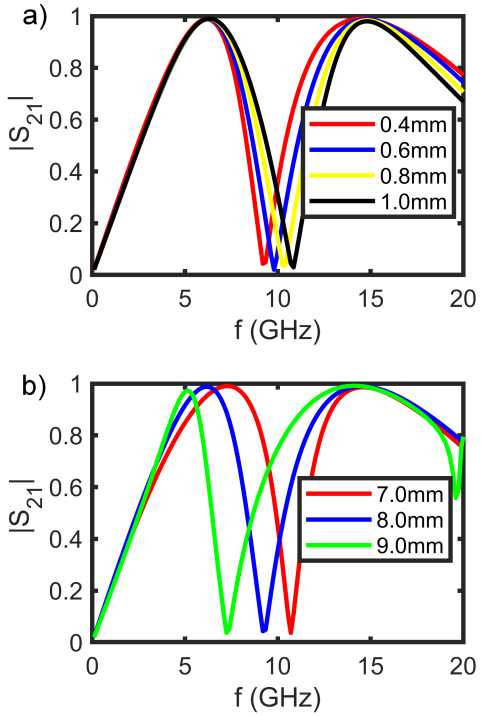

FIG. 3. Transmission spectra for different strip widths w_1 (a) and lengths l_1 (b) of the constituent square loop. The results have been obtained by full wave simulations. In the simulations we assumed copper as the metal, fr-4 as the dielectric substrate and a thickness of the dielectric substrate to be 0.1mm. We assumed the geometrical parameters D=10mm, w_2=0.1mm and w_3=2.5mm. In (a) l_1=8mm and in (b) w_1=0.4mm.

we can expect from Eq. (2), (4) and (5) that the bandstop frequency f_s increases slightly with the increase of w_1 and f_s shifts significantly to a lower frequency with the increase of l_1.

III. ANALYSIS MODEL VALIDATION BY FULL WAVE SIMULATION RESULTS

Fig. 3 shows full wave simulation results of the frequency response of the double square slot metasurface for different strip widths w_1 and lengths l_1 of the square loop. The bandstop frequency f_s shifts to a higher value when w_1 increases and f_s shifts significantly to a lower value when l_1 increases as expected above. Fig. 4 shows full wave simulation results of the transmission characteristics of the proposed FSS for different values of strip widths w_2 (a)

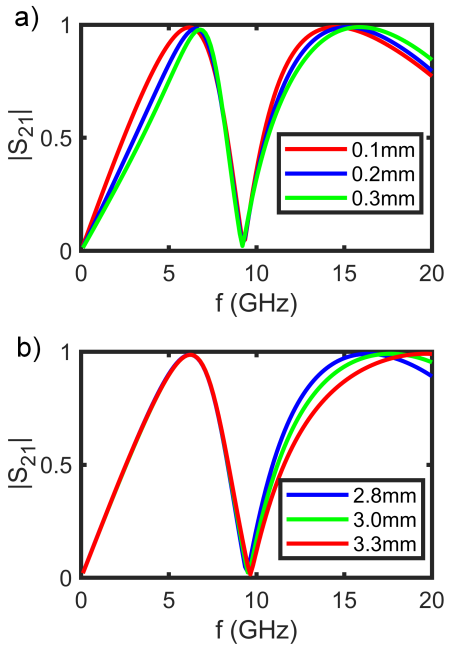

FIG. 4. Transmission spectra for different strip widths w_2 (a) and slot widths w_3 (b) of the constituent square slot. The results have been obtained by full wave simulations. We assumed the geometrical parameters D=10mm, l_1=8mm and w_1=0.4mm. In (a) w_3=2.5mm and in (b) w_2=0.1mm.

and slot widths w_3 (b) of the constituent square slot. As seen, the bandstop frequency f_s does not shift when the geometrical parameters of the constituent square slot change. Through the simulation results in Fig. 3 and Fig. 4, one can see that the bandstop frequency is tunable by changing the geometrical parameters of the constituent square loop and it is not dependent on the parameters of the constituent square slot. This coincides with the analytical predictions in Eq. (2). It is a good evidence that confirms the validity of our analysis model inwhich the double square slot is considered as the parellel combination of the constituent square loop and the constituent square slot. Additionally, from the full wave simulation results Fig. 3(b) and Fig. 4(b), one can also notice that the the lower and upper bandpass frequencies are individually tunable by changing the design parameters of the double square slot. The lower bandpass frequency f_{p1} is tunable by changing the length of the constituent square loop l_1 and the upper bandpass frequency f_{p2} is tunable by changing the strip width of the constituent square slot w_3.

The surface current distribution of the double square slot FSS is illustrated in Fig. 5. Fig.

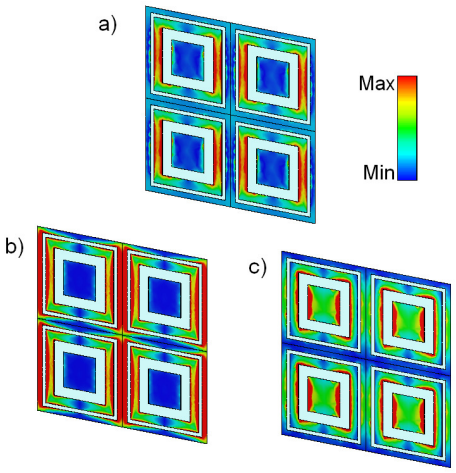

FIG. 5. Surface current distribution of the double square slot FSS at the bandstop frequency (a) and at the lower (b) and upper (c) bandpass frequencies, respectively. The results have been obtained by full wave simulations. The bandstop and bandpass frequencies are all chosen from the trasmission characteristics of the double square slot which is similar as in Fig. 3(a). Here, we assumed the geometrical parameters of the double square slot D=10mm, l_1=8mm, w_1=1.0mm, w_2=0.6mm and w_3=2.5mm. From the full wave simulation results, we chose the bandstop frequency 10.9GHz (a), the lower bandpass frequency 7.5 GHz (b) and the upper one 18GHz (c).

5(a) shows the surface current distribution at the bandstop frequency of the double square slot and Fig. 5(b) and (c) show the surface current distributions at the lower and upper bandpass frequencies, respectively. It is clear in Fig. 5(a) that at the bandstop frequency the surface current mainly distributes along the constituent square loop and it is considerably weak outside the constituent square loop. However, as seen in Fig. 5(b) and (c), the surface current distributes not only along the constituent square loop, but also along the constituent square slot. According to Fig. 5, we can see that it is the constituent square loop that mainly contributes to the resonance of the double square slot at the bandstop frequency and the resonances at the two bandpass frequencies are affected by both the constituent square loop and the square slot. The surface current distributions at the single stopband and the double passbands are in agreement with the analytical predictions from Eq. (2) and Eq. (3).

IV. CONCLUSION

In conclusion, we proposed an analysis model of a double square slot FSS considering its element as a parallel connection of the constituent square loop and the constituent square slot. While it is well known that the double square loop can be decomposed into two different square loops, the double square slot cannot be decomposed into two different square slots, instead it can be decomposed into square slot and square loop. Our analysis agrees with the known knowledge that the double square slot has dual passbands and inbetween single stopband and predicts crucial factors for tuning the inbetween stopband. The single bandstop frequency depends only on parameters of the constituent square loop and it does not depend on those of the constituent square slot. The single bandstop frequency is tunable by changing the length and strip width of the constituent square loop and it is not variable when changing the strip width and slot width of the constituent square slot. The predictions have been verified by full wave simulation results. Additionally, the simulation results show that two bandpass frequencies of the double square slot FSS are individually tunable by changing the length of the constituent square loop and the slot width of the constituent square slot, respectively. For its single layer structure, the proposed double square slot FSS can be ultrathin and in the simulations, a thickness of 0.1 mm which is of the order of $\lambda/300$ has been demonstrated. Despite in this paper we considered exemplary the square shape, our analytical model can be applied to other ring shapes including the annular ring shape as in [39].

DATA AVAILABILITY STATEMENT

The data that support the findings of this study are available from the corresponding author upon reasonable request.

CONFLICTS OF INTEREST

There are no conflicts of interest to declare.

---

[1] B. A. Munk, *Frequency Selective Surfaces - Theory and Design* (John Wiley and Sons, New York, 2000).

[2] W. Li, C. Wang, Y. Zhang, and Y. Li, "A miniaturized frequency selective surface based on square loop aperture element," Int. J. Antennas Propag. **2014**, 701279 (2014).

[3] X. D. Hu, X. L. Zhou, L. S.Wu, L. Zhou, and W. Y. Yin, "A miniaturized dual-band frequency selective surface (FSS) with closed loop and its complementary pattern," IEEE Antennas and Wireless Propag. Lett. **8**, 1374–1377 (2009).

[4] X. J. Sheng, J. J. Fan, N. Liu, and C.B. Zhang, "A miniaturized dual-band FSS with controllable frequency resonances," IEEE Microw. Wireless Compon. Lett. **27**, 915–917 (2017).

[5] P. C. Zhao, Z. Y. Zong, W. Wu, and D. G. Fang, "A convoluted structure for miniaturized frequency selective surface and its equivalent circuit for optimization design," IEEE Trans. Antennas Propag. **64**, 2963–2970 (2016).

[6] R. R. Xu, H. C. Zhao, Z. Y. Zong, and W. Wu, "Dual-band capacitive loaded frequency selective surfaces with close band spacing," IEEE Microw. Wireless Compon. Lett. **18**, 782–784 (2008).

[7] E. Zanganeh, M. Fallah, A. Abdolali, and N. Komjani, "New approach to design dual-band frequency selective surface based on frequency response tunning of each individual layer," Microw. Opt. Technol. Lett. **58**, 1423–1429 (2016).

[8] M. Li and N. Behdad, "A third-order bandpass frequency selective surface with a tunable transmission null," IEEE Trans. Antennas Propag. **60**, 2109–2113 (2012).

[9] A. Ray, M. Kahar, S. Biswas, D. Sarkar, and P. P. Sarkar, "A dual tuned complementary structure frequency selective surface for WLAN applications," J. Microw., Optoelectron. Electromagn. Appl. **11**, 144–152 (2012).

[10] R. R. Xu, Z. Y. Zong, and W. Wu, "Low-frequency miniaturized dualband frequency selective surfaces with close band spacing," Microw. Opt. Technol. Lett. **51**, 1238–1240 (2009).

[11] B. Li and Z. Shen, "Three-dimensional bandpass frequencyselective structures with multiple transmission zeros," IEEE Trans. Microw. Theory Tech. **61**, 3578–3589 (2013).

[12] J. Romeu and Y. R. Samii, "Fractal fss: A novel dualband frequency selective surface," IEEE Trans. Antennas Propag. **48**, 1097–1105 (2000).

[13] B. Li and Z. Shen, "Dual-band bandpass frequency-selective structures with arbitrary band ratios," IEEE Trans. Antennas Propag **62**, 5504–5512 (2014).

[14] M. Salehi and N. Behdad, "A second-order dual X-/Ka-band frequency selective surface," IEEE Microw. Wireless Compon. Lett. **18**, 785–787 (2008).

[15] F. Costa, S. Genovesi, and A. Monorchio, "On the bandwidth of high-impedance frequency selective surfaces," IEEE Antennas Wireless Propag. Lett **8**, 1341–1344 (2009).

[16] F. Costa, A. Monorchio, and G.Manara, "Analysis and design of ultra thin electromagnetic absorbers comprising resistively loaded high impedance surfaces," IEEE Trans. Antennas Propag. **58**, 1551–1558 (2010).

[17] G. H. H. Sung, K. W. Sowerby, M. J. Neve, and A. G. Williamson, "On the bandwidth of high-impedance frequency selective surfaces," IEEE Antennas Propag. Mag. **48(5)**, 29–37 (2006).

[18] A. Pirhadi, F. Keshmiri, M. Hakkak, and M. Tayarani, "Analysis and design of dual band high directivity EBG resonator antenna using square loop FSS as superstrate layer," Prog. Electromagnet. Res. **70**, 1–20 (2007).

[19] M. L. Li, Z. X. Yi, Y. H. Luo, B. Muneer, and Q. Zhu, "A novel integrated switchable absorber and radiator," IEEE Trans. Antennas Propag. **64**, 944–952 (2016).

[20] J. Y. Sze, C. I. G. Hsu, Z. W. Chen, and C. C. Chang, "Broadband CPW-fed circularly polarized square slot antenna with lightening-shaped feedline and inverted-L grounded strips," IEEE Trans. Antennas Propag. **58**, 973–977 (2010).

[21] F. Bayatpur and K. Sarabandi, "Single-layer high-order miniaturizedelement frequency-selective surfaces," IEEE Trans. Antennas Propag. **56**, 774–781 (2008).

[22] D. Ferreira, R. F. S. Caldeirinha, I. Cuinas, and T. R. Fernandes, "Square loop and slot frequency selective surfaces study for equivalent circuit model optimization," IEEE Trans. Antennas Propag. **63**, 3947–3955 (2015).

[23] Z. Yao, S. Xiao, Z. Jiang, L. Yan, and B. Z. Wang, "Analog absorber based on quasi-single-layer FSS," IEEE Antennas Wireless Propag. Lett. **19**, 591–595 (2020).

[24] T. K. Chang, R. J. Langley, and E. A. Parker, "An active square loop frequency selective surface," IEEE Microw. Guided Wave Lett. **3(10)**, 387–388 (1993).

[25] R. J. Langley and E. A. Parker, "Equivalent-circuit model for arrays of square loops," Electron. Lett. **18**, 294–296 (1982).

[26] F. Costa and A. Monorchio, "A frequency selective radome with wideband absorbing properties," IEEE Trans. Antennas Propag. **60**, 2740–2747 (2012).

[27] J. Yang and Z. X. Shen, "A thin and broadband absorber using double-square loops," IEEE Antennas Wireless Propag. Lett. **6**, 388–391 (2007).

[28] M. Li, S. Q. Xiao, Y. Y. Bai, and B. Z. Wang, "An ultrathin and broadband radar absorber using resistive FSS," IEEE Antennas Wireless Propag. Lett. **11**, 748–751 (2012).

[29] G. H. Dadashzadeh, M. H. Amini, and A. R. Mallahzadeh, "Equivalent circuit model for square ring slot frequency selective surface," Int. J. Antennas Propag. **3**, 23–31 (2014).

[30] D. Wang, W. Che, Y. Chang, K. S. Chin, and Y. L. Chow, "A low-profile frequency selective surface with controllable triband characteristics," IEEE Antennas Wireless Propag. Lett. **12**, 468–471 (2013).

[31] S. Genovesi, F. Costa, and A. Monorchio, "Low profile array with reduced radar cross section by using frequency selective surfaces," IEEE Trans. Antennas Propag. **60**, 2327–2335 (2012).

[32] K. R. Jha, G. Singh, and R. Jyoti, "A simple synthesis technique of single-square-loop frequency selective surface," Prog. Electromagn. Res. B **45**, 165–185 (2012).

[33] Chol-Song Ri, Hye-Jong Yun, Song-Jin Im, and Yong-Ha Han, "Bandwidth analysis of microwave metamaterial absorber with a resistive frequency selective surface by using an equivalent circuit model," AEU-Int. J. Electron. Commun. **148**, 154160 (2022).

[34] Y. Shang and Z. Shen, "On the design of single-layer circuit analog absorber using double-square-loop array," IEEE Trans. Antennas Propag. **61**, 6022–6029 (2013).

[35] A. E. Yilmaz and M. Kuzuoglu, "Design of the square loop frequency selective surfaces with particle swarm optimization via the equivalent circuit model," Radio Engineering **18**, 95–102 (2009).

[36] M. Rahzaani, G. Dadashzadeh, and M. Khorshidi, "New technique for designing wideband one layer frequency selective surface in X-band with stable angular response," Microw. Opt. Technol. Lett. **60(9)**, 2133–2139 (2018).

[37] A. Firouzfar, M. Afsahi, and A. A. Orouji, "Novel straightforward procedure to design square loop frequency selective surfaces based on equivalent circuit model," AEU-Int. J. Electron. Commun. **119**, 153164 (2020).

[38] Y. Yang, X. H. Wang, and H. Zhou, "Dual-band frequency selective surface with miniaturized element in low frequencies," Prog. Electromagn. Res. Lett. **33**, 167–175 (2012).

[39] Y. Cheng and H. Liu, "A novel concentric annular-ring slot dual-band circularly polarized microstrip antenna," Int. J. Antennas Propag. **7560567**, 1–8 (2018).

[40] Z. Xia, F. Liu, X. Tang, X. Cao, and Q. Cai, "A compact fss with dual passbands and wide stopband," AEU-Int. J. Electron. Commun. **16**, 1–6 (2019).

[41] Y. Xu and M. He, "Design of multilayer frequency-selective surfaces by equivalent circuit method and basic building blocks," Int. J. Antennas Propag. **2019**, 9582564 (2019).